INDERSCIENCE PUBLISHERS
Linking academia, business and industry through research

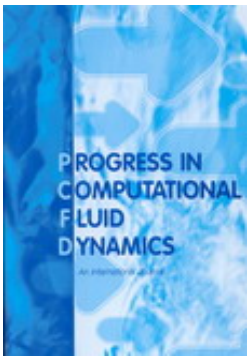

Progress in Computational Fluid Dynamics, An International Journal

ISSN online: 1741-5233 - ISSN print: 1468-4349
https://www.inderscience.com/pcfd

Computational analysis of high speed super-cavitating projectiles for reduction of hydrodynamic drag using cavitator optimisation

Rohini Dharmaraj, Amarkarthik Arunachalam, Sivaraj Gurunath, Haran Pranatharthy Athmanathan

DOI: 10.1504/PCFD.2024.10064808

Article History:

Received:	23 August 2023
Last revised:	25 November 2023
Accepted:	13 April 2024
Published online:	06 January 2025

Computational analysis of high speed super-cavitating projectiles for reduction of hydrodynamic drag using cavitator optimisation

Rohini Dharmaraj*, Amarkarthik Arunachalam and Sivaraj Gurunath

Department of Aeronautical Engineering,
Bannari Amman Institute of Technology,
Sathyamangalam, Erode – 638401, India
Email: rohinidharmaraj90@gmail.com
Email: amarkarthik@bitsathy.ac.in
Email: togsiva@gmail.com
*Corresponding author

Haran Pranatharthy Athmanathan

Department of Aeronautical Engineering,
Park College of Engineering and Technology,
Kaniyur, Coimbatore, 641659, India
Email: ap_haran@rediffmail.com

Abstract: The goal of the paper is the computational analysis of cavitator shape with respect to the forebody of the projectile, which recommends the supercavitation phenomenon. The main target is to provide a phase-changing mechanism for two-phase fluid flow simulation. By employing ANSYS Fluent for disk cavitator, a steady and incompressible two-phase fluid has been analysed, and during the simulation, cavitation is observed. For the designed geometry of the forebody of the projectile, multiphase flow has been chosen, for varying cavitation number of 0.1–0.01, to optimise the disk cavitator's diameter to begin an effective creation of supercavity. The computational analysis of the result displays about the cavity formation, cavity growth, cavity body, and drag prediction for the projectile. To optimise the cavitator diameter, which plays a key role in the formation of supercavitation, 3 mm cavitator disk diameter with a disk to projectile diameter ratio of 0.375 generates the minimum hydrodynamic drag.

Keywords: super-cavitation projectile; disk cavitator; hydrodynamics; skin friction drag; multiphase flow.

Reference to this paper should be made as follows: Dharmaraj, R., Arunachalam, A., Gurunath, S. and Athmanathan, H.P. (2025) 'Computational analysis of high speed super-cavitating projectiles for reduction of hydrodynamic drag using cavitator optimisation', *Progress in Computational Fluid Dynamics*, Vol. 25, No. 1, pp.1–15.

Biographical notes: Rohini Dharmaraj is an Assistant Professor in the Department of Aeronautical Engineering at Bannari Amman Institute of Technology. She is pursuing a part-time PhD at Anna University, with a focus on hydrodynamics. Her current research involves underwater projectiles.

Amarkarthik Arunachalam is a Professor in the Department of Mechanical Engineering at Bannari Amman Institute of Technology. His research area is ocean wave energy, and he serves as a guiding supervisor. He has received funding for the completion of the 'Design, development, and testing of a novel double-acting power take-off system for ocean wave energy conversion' project.

Sivaraj Gurunath is an Associate Professor in the Department of Aeronautical Engineering at Bannari Amman Institute of Technology. His research area is vehicle aerodynamics. He has two granted patents.

Haran Pranatharthy Athmanathan is the Director at the Park Research Center with extensive experience in aerospace propulsion, turbomachinery, and combustion. He serves as a guiding supervisor and has completed seven sponsored projects. From 1973 to 1994, he worked as a Chief Engineer in Indian Air Force, and from 1994 to 2007, he served as a Group Director at GTRE.

1 Introduction

Cavitation has been discovered in numerous different applications of hydrodynamics, namely hydrofoils, spillways, and pumps. In almost all of the examples, cavitation is shown to have detrimental impacts, including decreased pump efficiency, decreased hydrofoil lift, and material damage. Cavitation may be irresistible in the aforementioned cases. Therefore, there is a requirement for the minimisation of the effects of cavitation or for taking advantage of the phenomenon. Supercavitation can be a feasible solution in the latter case. There are many technologies that have been created to utilise supercavitation phenomena to their advantage. Super-cavitating propellers, hydrofoils, and hydraulic turbines are examples of super-cavitating devices. Out of these examples, there are many that, when cavitation is unavoidable, take advantage of the tendency to use the steadiness of supercavitation (Knapp et al., 1970).

When the size of the cavity entirely covers the undersea object, there is an appearance of the supercavitation phenomenon with a considerably low number. In this regime, in contrast to other forms of cavitation, the main flow and the cavitation region generally have a distinct interface between them. Extremely low cavitation numbers are required for the occurrence of super-cavitation. Boosting the free stream velocity or elevating the cavity pressure through cavity ventilation are two of the various ways of accomplishing this. An accurately placed cavitator with a well- considered edge ensures the formation of a clean cavity close to the axisymmetric body. In order to decrease the hydrodynamic drag, it is extremely important to have a cavitator with a relatively small diameter in comparison to the axisymmetric body.

Recent years have witnessed an inclination toward supercavitation research, owing to its potential for vehicle handling and drag reduction (Hrubes, 2021). A method called free stream based on the potential flow theory has been created by Yao-Tsu and Wang (1963) to forecast the cavitation dynamics. However, as the potential flow analysis does not take into account the effects of viscosity and turbulence, it is insufficient as a predictive framework. Tassinleger and Ceccio (1998) optimised the projectile using an axisymmetric model in order to determine where the two- dimensional laminar boundary layer parted. By using the methods of Thwaites and Stratford, the cavity detachment upstream of the boundary layer split was forecast, and the boundary layer partition was noticed. When the flowing liquid gets separated from the solid surface, cavitation occurs, resulting in the creation of a vapour coating that is often stable. When a projectile moves through water fast enough, there is acceleration in flow in certain locations around the nose, which drops the static pressure below the vapour pressure and leads to the creation of a vapour cavity (Brennen, 1995).

Generally, as soon as the projectile has passed, these cavities seal up. On the other hand, with sufficient speed and the appropriate design elements, for example, a flat nose tip and a slender conical body, a cavity can be formed that will enclose the entire body and remain for a very long period of time after the projectile has passed (Chou, 1974; Jagadeshwar et al., 2021). Lotan and Alon (2022) studied the creation of supercavitation bubbles over cylinderical bodies, travelling underwater in a pool, which have a free, unbounded surface. The effect of six various geometries of the cavitator on the start progress, and dimensions of the formed bubble was investigated in relation with the flow speed and the cavitation number. The outcomes were put into comparisons with those which were discovered in a duct flow. A projectile travelling at a high speed through supercavitation moves forward inside the cavity; however, it turns due to insufficient water entry. This rotation results in repeated contact between the cavity wall and the projectile tail. Hits have an effect on both the projectile's trajectory and motion stability (Salil and Rudra, 2000).

There is the possibility of both naturally occurring and man-made supercavities. A natural supercavity is formed when the liquid has hydrodynamic pressure reduction that encircles a solid mass, and there is the generation of an artificial supercavity utilising gas with vents from several sources. This gas can either aid the expansion of a small natural cavity or can create a cavity in a zone with low-pressure liquid, which, at a significantly lower projectile's pace, enables supercavitation. There are a few potential sources for ventilation gas, including the projectile's compressed gas, exhaust gases from its propulsion system, entrained air from above the water's surface, and propulsion exhaust gases (Peter et al., 2011).

In their research, Chang et al. (2018) examined only natural supercavitation. Cavitating flow close to the free surface is demanding and can generate novel approaches for high-speed surface cruising. For analysis, Van-Tu and Warn-Gyu (2022) used an axisymmetric projectile in his experiment. To evaluate the super-cavitating flow around projectiles moving at high subsonic to supersonic speeds statistically, a totally compressible multiphase flow with phase change is used. Dong-Hui et al. (2022), in his paper, simulated a multiphase flow field with supercavitation, which is caused by two projectiles, which were fired successively underwater and cross-media (water-entry and water-exit). Particularly, there is analysis of the impact of the interaction between supercavities, which are induced by two projectiles. Additionally, an examination was done, which demonstrates the way in which the evolution of the supercavity put an impact on the mobilisation of the two projectiles. Gugulothu (2020) established the accuracy of the numerical method by contrasting the analysis outcomes of the super-cavitating flow around an underwater projectile with the experimental data provided in the literature. A single fluid model was used by Seongjin and Gihun (2021) to specify the vapour-liquid flow, which is believed to be a homogeneous mixture; merely one set of equations is mandatory for the simulation of the cavitating flow. Van-Duyen et al. (2022) systematically investigated how the properties of a ventilated super cavity are affected by the shape of the cavitator. These properties include behaviour of pressure, demand for ventilation, and super cavity

deformation because of the gravity under distinct flow circumstances. So, a homogeneous mixture model, including the influence of vapour generation, a semi-implicit pressure correction technique for compressible two-phase flows, and an immersed boundary methodology to apply particular conditions of velocity to a mobile solid surface.

There are underwater weapons, including torpedoes, that are restricted to a maximum speed of 40 knots by the noticeable drag that is created due to the skin friction on the hull skin. For acoustics and hydrodynamic efficiency, low speed is an advantage. A torpedo is a weapon that is self-propelling in nature and has an explosive warhead that is launched above or below the surface of water. Except for a few torpedoes propelled by rocket engines and projectiles not containing any explosives, which are launched by guns, a propeller propels most of the torpedoes under the water. Water resistance will slow down the bullet rapidly when it is shot from a pistol into water. Compared to a standard missile, the drag experienced by the torpedo and projectile is very high, as water has a much higher density compared with air. These have a restricted range, resulting in a steady decline in performance. Speed of the conventional under water projectile is very less due to the fact that water is denser than the air, which provides more resistance. For compensation, underwater projectiles are designed in the way that they are more hydrodynamically efficient and streamlined, permitting them to have greater speeds and travel farther underwater. Today, the global navy is expecting submerged machines that are able to travel faster than the present speed of 30–40 knots. Some special technology is required to attain high speed and low drag. Under conventional hydrodynamic operating conditions, there is no realisation of high speed. Super-cavitation aids a rise in maximum speed by lowering the drag of an underwater body (Hrubes, 2021). Because of their unique capabilities, the analysis of supercavitation projectiles is crucial. It is important to understand and analyse these projectiles for military applications. Naval applications of supercavitation projectiles are, their use for high-speed underwater travel. It is essential to analyse them for optimising military strategies, anti-submarine warfare, and submarine defenses.

A number of researchers have reported anticipating super-cavitating flows by making use of artificial cavitating in the incompressible and compressible. There is availability of a few research, which is based on the natural cavitation. To analyse vapour density formation and cavity closure point, employing natural cavitation is lagging *3D* (three-dimensional) a numerical analysis. To improve the formation of supercavity, *3D* model bullet needs computational analysis research. The research paper is based on the process of optimising the Cavitation for the underwater projectiles, to attain the natural cavitation, and to drop the skin fraction drag, that acts on the vehicle. The research has been conducted to decrease the skin fraction drag, which acts on the super-cavitating vehicle by forming vapour density. This is the novelty of the analysis of super-cavitating underwater projectiles employing a disk cavitator, which offers enhanced pace, control, and adoptability. To attain this, a disk cavitator is positioned ahead of the projectile with the goal to facilitate the changeover process in density when the simulation of two-phase fluid flows happens. Hence, the total drag that acts on the super-cavitating vehicle is minimised as a result of the reduction in skin friction drag. This strategy contributes to improvement in civilian as well as military applications of underwater technology.

2 Cavitator

Selecting a cavitation that is perfectly sized for supercavitation vehicle is a crucial step in designing the super-cavitating body. Cavitator has to be positioned infront of the projectile, acting as a nose of the projectile to begin the cavity, and close to the nose of the projectile, the creation of clean cavity is ensured. Because of a realtive small diameter of the cavitator, it is extremely significant to place the cavitator with respect to the projectile body. During its travel through the water, the cavitator in a super-cavitating vehicle is responsible for the start, maintenance and the control of the gas cavity around the vehicle.

Disk cavitator, cone cavitator and ring cavitator are included in the three forms of cavitation. Figure 1 depicts disk cavitator, taken into account in the research, as it limits the entry of water molecules inside the projectile's nose. To attain this, the projectile is created with a flat face, known as disk cavitator, normal to the body's axis. Selection of the cavitator diameter for the given body geometry is crucial for dropping the skin friction drag along with the overall body drag. This work considers the thickness of the flat plate to be ignorable ahead of the projectile's surface.

Figure 1 Disk cavitator for gun launched projectiles

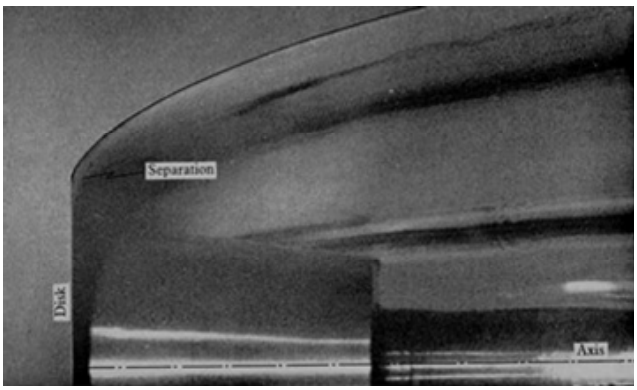

Source: Brennen (1970)

2.1 Cavitation model

When the local pressure is decreased to a value close to the saturation vapour pressure of the liquid, there is an occurrence of a dynamic phenomenon known as cavitation (Brennen, 1995). During the creation of the vapour bubbles or cavities, there is a visual experience of cavitation. The

cavitation number is the fundamental parameter that depicts cavitation, and it is defined as k. The fundamental parameter describing the cavitation is the cavitation number equation (1), defined as

$$k = \frac{P_0 + \rho g h - P_b}{\frac{1}{2}\rho V_0^2} \quad (1)$$

where the cavitation number is represented by k, the free steam static pressure by P_0, the saturation liquid vapour pressure by P_b, the liquid's density by ρ, the submersion depth by h, and the free stream velocity by V_0. When there is a minimum pressure in the flow equal to the saturation pressure, there is an assumption of the occurrence of cavitation under most circumstances (Hrubes, 2001).

At low cavitation numbers, a solid boundary can have a large cavity attached to it, and in extreme cases, a body can be entirely enveloped by the cavity, which is known as supercavitation (Peter et al., 2011). There is a great reduction in the drag of the body, which the cavity surrounds, when there is an occurrence of supercavitation (Chang et al., 2018). The factor responsible for this is skin friction drag, relying on the fluid's viscosity being lowered because of the vapour pockets around the body. One of the two ways can be used to maintain a supercavity: by moving the body at a fast pace, the vaporisation of the water occurs close to the nose of the body, and the supply of gas to the cavity is closely monitored at ambient pressure (Kunz et al., 1999). This research uses Natural Super Cavitation to decrease skin fraction drag. By utilising mass transfer modelling, there is exchange between the liquid and vapour phases.

Optimising the diameter of the disk cavitator to begin effective supercavitation is the main aim. As the vehicle travels forward, this optimisation aids in the formation of the beginning bubble and supercavity. Thereafter, the cavity encases the vehicle, decreasing water contact with the vehicle's surface and hence reducing drag. This shape optimisation is achieved by two-phase fluid flow simulation. Simulation and analysis of a steady, two-phase fluid flow have been carried out. In the beginning, two-phase fluid flow analysis is done over the disk cavitator alone to find the supercavitator generation. Once the supercavitation formation is identified, the disk is positioned in the projectile's forebody and analysed for variable cavitation number (k), 0.1 to 0.01.

2.2 Steps for finalising the cavitator design

- To identify the creation of cavitation, cavitator alone and the length of the projectile were analysed in the beginning.
- For supercavitation number 0.1, the cavitator's nose was optimised.
- To identify the creation of cavities over the surface, an additional step using a cavitator comparator and projectile analysis was taken.
- For the changing cavitation number from 0.1 to 0.01 and the flow pattern, the projectile geometry, cavity formation and cavity envelope predicted from the CFD analysis, cavitation research proceeded.
- Based on the total drag curve, the cavitator disk diameter was optimised by employing the analysis of the CFD outcomes.

3 Computational study

To optimise the cavitator, the computational analysis was used with respect to the projectile's body and, hence, put into comparison with the experimental outcome of Brennen (1969). Disk cavitators aid in starting the natural supercavitation, which is a solution to overcome the total drag, which acts on the super-cavitating projectile.

The cavitation model in computational analysis has its basis in the model named 'full cavitation model', which was developed by Ashok et al. (2002). All the first-order effects, that is, phases change, bubble dynamics, and turbulence fluctuations are taken into consideration. It is always preferable to use the cavitation model and the mixture multiphase model together as a solution for cavitation. Considerable slip between phases can be spotted when the slip velocity is turned on. Large bubble growth is not allowed in this flow because of the high level of turbulence, leaving gravity unimportant and nullifying the need for a solution for slip velocity. Supercavitation occurs at a specific number, 0.1, and this happens when there is a fall in the local pressure below the saturation vapour pressure. For this reason, in the cavitation dialog box, the value of saturation vapour pressure, derived from the steam table, will be fixed.

Significant insights into gun-launched projectiles are provided by optimising the design of cavitators. Firstly, in this analysis it focuses on the importance of cavitator in maintaining a stable supercavity formation, which is crucial for decreasing drag and allowing high-speed underwater travel. This focuses on the importance of the selection of material and caviator geometry to attain this target. Moreover, the analysis highlights the significant streamlined contours and this helps to decrease the flow separation and improve the performance of the cavitator. The flow properties around the cavitator assists in modifying designs for enhanced stability and maneuverability while travelling underwater. Finally, the research focuses on the necessity of further study to enhance designs of cavitator, making sure that they effectively employ the principle of supercavitation for refined projectile performance in gun-launched applications. All these findings display a base for modifying cavitator technology for underwater fast projectiles.

3.1 Geometry of cavitator disk

The disk cavitator has a key role to play in the creation of a supercavity, which begins at the front of the projectile. A supercavity must be formed at the nose to take full

advantage of the drag reduction available, so it encases the body entirely. This is achieved by designing disk cavitation with a flat face normal to the body's axis, as illustrated in Figure 2. In this task, the length of the projectile and angle used has been selected from Peter et al. (2011) and the diameter of the flat plate varies from 1mm to 8mm. The detailed dimensions are represented in Table 1.

Figure 2 Schematic diagram of geometry of cavitator disk (see online version for colours)

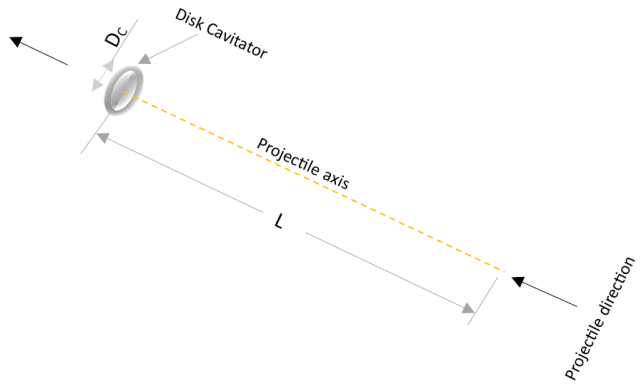

3.2 Geometry of disk ahead of projectile body

There are certain aspects of the current models of mathematics that are suitable for engineering applications. There is a typical assumption of constant pressure along the free streamline by them, which gets apart from the body for a specific distance. The mathematical conditions that are used to seal up the cavity do not have any impact on the forces acting on it or the shape of the cavity near the body. Hence, the primary disposable parameter is the cavity pressure, normally assumed to be water vapour pressure (Gadd and Grant, 1965). Bullets, rockets, and missiles are included in many applications, which are all solid bodies of revolutions and for which designing a nose cone geometrical shape, encountering minimum resistance to quick motion through the fluid material, is required. A number of aerodynamic nose Cone designs are available currently. Figure 3 illustrates one of the projectile designs. Selected for this research. From Peter et al. (2011), the projectile design and configuration has been referred to.

Figure 3 Schematic diagram of disk ahead of projectile body (see online version for colours)

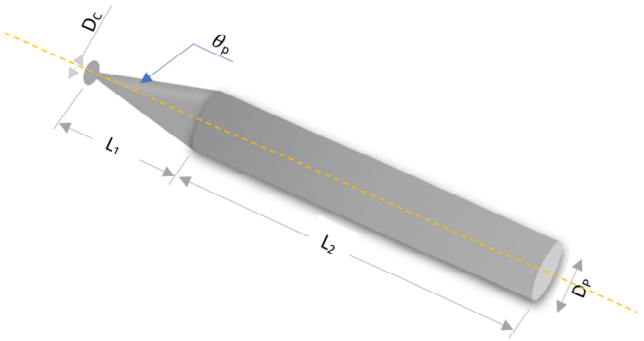

The shape of the projectile is fixed as a constant in this case, and a disk cavitator has a diameter varying from 1mm to 8mm. Table 1 represents the detailed dimensions.

Table 1 Dimension specification for cavitator disk with and without projectile

Specification	*Dimension*
Diameter of cavitator disk (*Dc*)	1 to 8 mm
Overall length of the projectile (*L*)	63 mm
Projectile cone length (L_1)	21 mm
Projectile body length (L_2)	42 mm
Projectile cone angle (θ_p)	12 deg

3.3 Mesh generation and boundary condition

There is the creation of a 3*D* domain as a single passage surrounding an object, with inlet at 5 *L* upstream, and here, *L* represents the projectile's length; exit is at 15 *L* downstream, whereas the domain's diameter is 10 *L*. Figure 4 illustrates the boundary conditions specified for the geometry. A fine computational structure was generated. First, the surface of the object was meshed using a mapped mesh. Close to the surface of the object, a fine mesh was created, while at the rest of the places, a coarse mesh was generated, as represented in Figure 5.

Figure 4 Domain and boundary condition (see online version for colours)

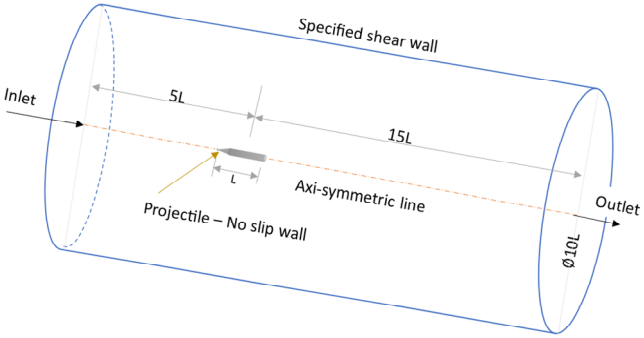

Figure 5 3D structured grid (see online version for colours)

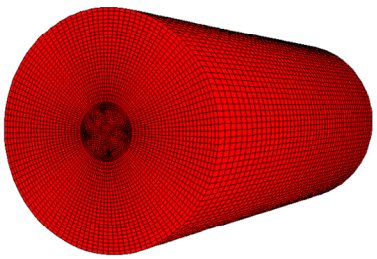

The term grid independence is used to describe the improved outcomes achieved by successfully employing small sizes of cells for the selected geometry. As the mesh becomes finer, the correct answer should be approached by calculation. Grid independence was carried out in order to establish the accuracy, dependency, and convergence of the numerical simulation. In the *k-ε* turbulence model, the

independence study is don. Simulation of supercavitation behind 3mm cavitation is done at a cavitation number k = 0.1, employing four distinct cell count of 0.040, 0.045, 0.050, and0, 0.055 million, and the C_D value was discovered to be 0.0791, 0.07, 0.0703 and 0.0707, respectively. No significant difference was observed in the coefficient of drag from 0.045 million cells to 0.055 million cells. From the utilisation of time and accurate outcome, the selection of 0.045 million cell counts was observed to be satisfactory for all simulations, as depicted in Figure 6 and Table 2 illustrates the grid independence study value.

Table 2 Grid independence check for 3 mm cavitator disk for number of cells and coefficient of drag

Number of cells (million)	C_D
0.040	0.0791
0.045	0.0700
0.050	0.0703
0.055	0.0707

In this super cavitation multiphase computational analysis, changing the mesh size and type of the element puts a significant impact on the outcomes of simulation. The domain is discretised by a finer mesh with greater detail, enabling the record of flow characteristics and complex features accurately. On the other hand, there is a rise in the computational load, requiring a considerable computer resources and lengthening durations of solution. But when computations are accelerated by a coarer mesh, there may be a loss of fine-scale flow phenomena, and may result in findings, that are less accurate. High-order elements, namely cubic or quadratic, are advantageous for the simulation of complex fluid behaviour, for they require fewer elements, and maintain efficiency accurately. In contrast, lower-order elements, for example, linear, are not very computationally demanding; however, they may require a finer mesh to achieve a similar precision.

In this cavitator analysis, A finer mesh encourages the solution to converge, and brings the numerical approximation closer to the actual fluid characteristics gradually. However, the presence of more components in this refinement increases the computational expenses. Although computing costs are reduced by coarer mesh, they can lead to numerical diffusion and dissipation effects; thus, it is necessary to select a mesh accurately for reliable CFD analyses. Therefore, it is essential to consider mesh size and element type accurately, so there is balance between computing efficiency and recording of intricacies of fluid dynamics, in order to perform reliable and accurate CFD simulations.

The multiphase analysis carried out using Y+ values and the Y+ value plays a role as a critical parameter in steady flow analysis for super-cavitating projectiles. It depicts the first grid cell's dimensionless distance from the wall to the viscous sublayer. In this flow analysis the Y+ value of 5 is analysed for the surface of the Cavitator for turbulence model of *k-ω*. This low Y+ value is used for the accurate prediction of the flow characteristics and distribution of pressure around the cavitator, in order to optimise the super-cavitating projectiles' design.

Boundary conditions employed in this research are Inlet-acts as a velocity inlet, and it's value is calculated using equation (1). Outlet-acts as a pressure outlet, Cavitator disk behind projectile's body-acts as a wall, with no slip condition, upper section-acts as a wall, has a certain shear, interior lines-act as an interior, and Centre line-acts as an interior line.

Figure 6 Grid independence study for cavitator disk for number of cells

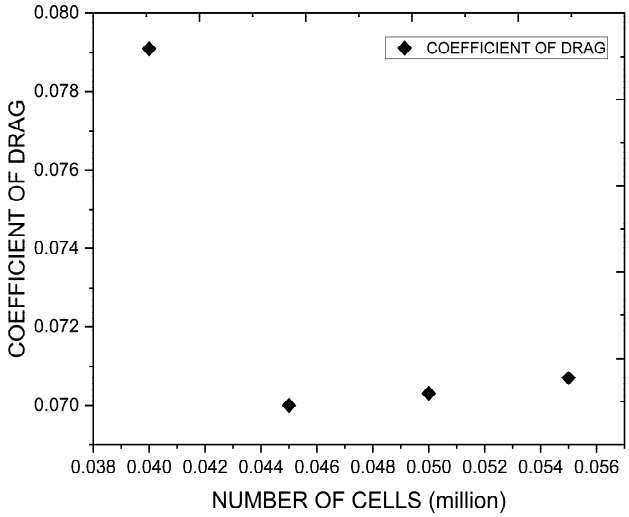

3.4 Governing equation

Over a disk cavitator, an ideal steady flow is developed for a computational model. Flat plate-shape assumptions were made with Ko et al. (1969) finite difference wake creation. The governing equations were the balance equations of momentum and the conservation of mass. The simple algorithm introduced by Patankar (1980) follows these. This conservative form has a demanding solution, whereas by applying Reynolds with the averaged Navier-Stokes (RANS) equation, calculations were simplified. The cavitation model has a successful application of this method. Mixture/multiphase flow equations are applied to illustrate the motions of liquid water and water vapour, which include the phase transition. The momentum and continuity equations developed for the mixture are as follows:

Conservative form of Continuity equation

$$\nabla \cdot \left(\rho \vec{V} \right) = 0 \tag{2}$$

Conservative form of X-momentum equation

$$\nabla \cdot \left(\rho u \vec{V} \right) = \frac{\partial p}{\partial x} + \frac{\partial \tau_{xx}}{\partial x} + \frac{\partial \tau_{yx}}{\partial y} + \frac{\partial \tau_{zx}}{\partial z} + \rho f_x \tag{3}$$

Conservative form of energy equation

$$\nabla\cdot\left[\rho\left(e+\frac{V^2}{2}\vec{V}\right)\right]=pq+\frac{\partial}{\partial x}\left(K\frac{\partial T}{\partial x}\right)-\frac{\partial(up)}{\partial x}+\frac{\partial\left(u\tau_{xx}\right)}{\partial x}+\frac{\partial\left(u\tau_{yz}\right)}{\partial y}+\frac{\partial\left(u\tau_{zx}\right)}{\partial z}+\rho\vec{f}\cdot\vec{V} \quad (4)$$

It is important to choose the turbulence model for solving the cavitation model. k-epsilon and k-omega were the two different kinds of turbulence models taken into consideration in this research work. The computing region has the conservative form of continuity and energy equation satisfied in it. Numerical calculations have been employed nearly close to the experimental conditions to make comparison with experimental outcomes by Brennen (1970). The flow under examination is considered having disturbances expanding only in spicy, not in time (Brennen, 1970). Pressure based solver and formation of absolute velocity is utilised. Application of this solver is restricted to the analysis of the cavitation model, while it is not possible to have cavity analysis with density-based solver. For analysis, the homogeneous mixture model is considered. The working medium is a single fluid, having a homogeneous mixture of two phases i.e. liquid and vapour, assumed by the multi-phase mixture model in FLUENT. The primary phase considered is water liquid medium for phase I, whereas water vapour is considered as a secondary for phase II. Schnerr-Sauer cavitation model was taken into account, vaporisation density, Pressure value selected from the steam table and for the 1m depth the analysis done the corresponding temperature, pressure, and saturated vapor pressure value is chosen from the steam table. In this analysis, 0.75 is a dispersion Prandtl number considered, and Prandtl number for energy and wall was 0.85. SIMPLE velocity -pressure coupling was taken into consideration. Because this solution method is much more rapid and employed for performing more iteration than the PISO and COUPLED. Due to its aggressive convergence behaviour, this solution method is suitable for the analysis of transient model, resulting in solving one set of RANS equations for the mixture fluid. This research uses a multiphase model to forecast the cavity creation and density of mixture. Initially, by selecting two distinct turbulent models, cavitation analysis is carried out for the disk cavitator. The result suggests that *k*-*ε* is less efficient as compared to the *k*-ω model. Therefore, there is a further analysis carried out, and represented in Table 3.

A stable equilibrium is reached over time in steady-state simulations with the flow parameters remaining constant. Where the flow remains constant and unchanging, they are suitable and provide precise outcomes of cavity length, skin friction drag and coefficient of drag. On the other hand, they may not be appropriate for cases, which involve quickly altering flow conditions or where there is a significant role of transient impacts.

Table 3 Coefficient drag value for turbulence model of *k*-*ε* and *k*-*ω*

Disk diameter in mm	*Coefficient of drag*	
	k-*ε*	*k*-*ω*
1	1.234	1.048
2	1.102	0.989
3	0.994	0.959
4	0.974	0.940
5	0.964	0.937
6	0.954	0.910
7	0.967	0.943
8	0.987	0.963

As steady-state simulations are computationally more efficient for the super cavitation disk cavitator analysis, steady state analysis sufficient for stable flow patterns. Contours of density were predicted from the steady state analysis using multiphase flow condition. While in the case of transient simulations, they demand more computational resources as the nature of the analysis is time-dependent. To summarise, the selection between steady-state and transient simulations is determined by the required level of accuracy and the type of flow. For steady, constant flow situations, steady-state simulations are a precise choice as they provide computational efficiency.

4 Results and discussion

For the cavitation number varying from 0.1 to 0.01, the disk cavitator alone and the disk cavitator ahead of the projectile model were analysed and confirmed with the literature Brennen (1970) cavitation model in ANSYS Fluent.

4.1 Case 1: super-cavitation behind a disk cavitator

Initially, analysis of the cut section of the 3D disk is carried out for a cavitation number of 0.1 and a Reynolds number of Re = 158 × 10^6. Figure 7 depicts the development of supercavity creation and cavity flow contour for varying cavitator diameters. The steady supercavity shape forms are found by applying equation 1 at a velocity of 44 m/s. For different disk cavitator diameters, CFD simulation is carried out. Supercavity length, cavity diameters, pressure drag, skin friction drag, and coefficient of drag value are established from the simulation. During the separation at a sharp projecting corner on a head form, the geometry of the cavity and the wetted surface pressure distribution are perfectly predicted by potential flow theory (Brennen, 1969).

Figure 7 Vapour density formation (mixture) for disk cavitator without projectile body (a) vapour density formation for 1 mm D_c (b) vapour density formation for 2 mm D_c (c) vapour density formation for 3 mm D_c (d) vapour density formation for 4 mm D_c (e) vapour density formation for 5 mm D_c (f) vapour density formation for 6 mm D_c (g) vapour density formation for 7 mm D_c (h) vapour density formation for 8 mm D_c (see online version for colours)

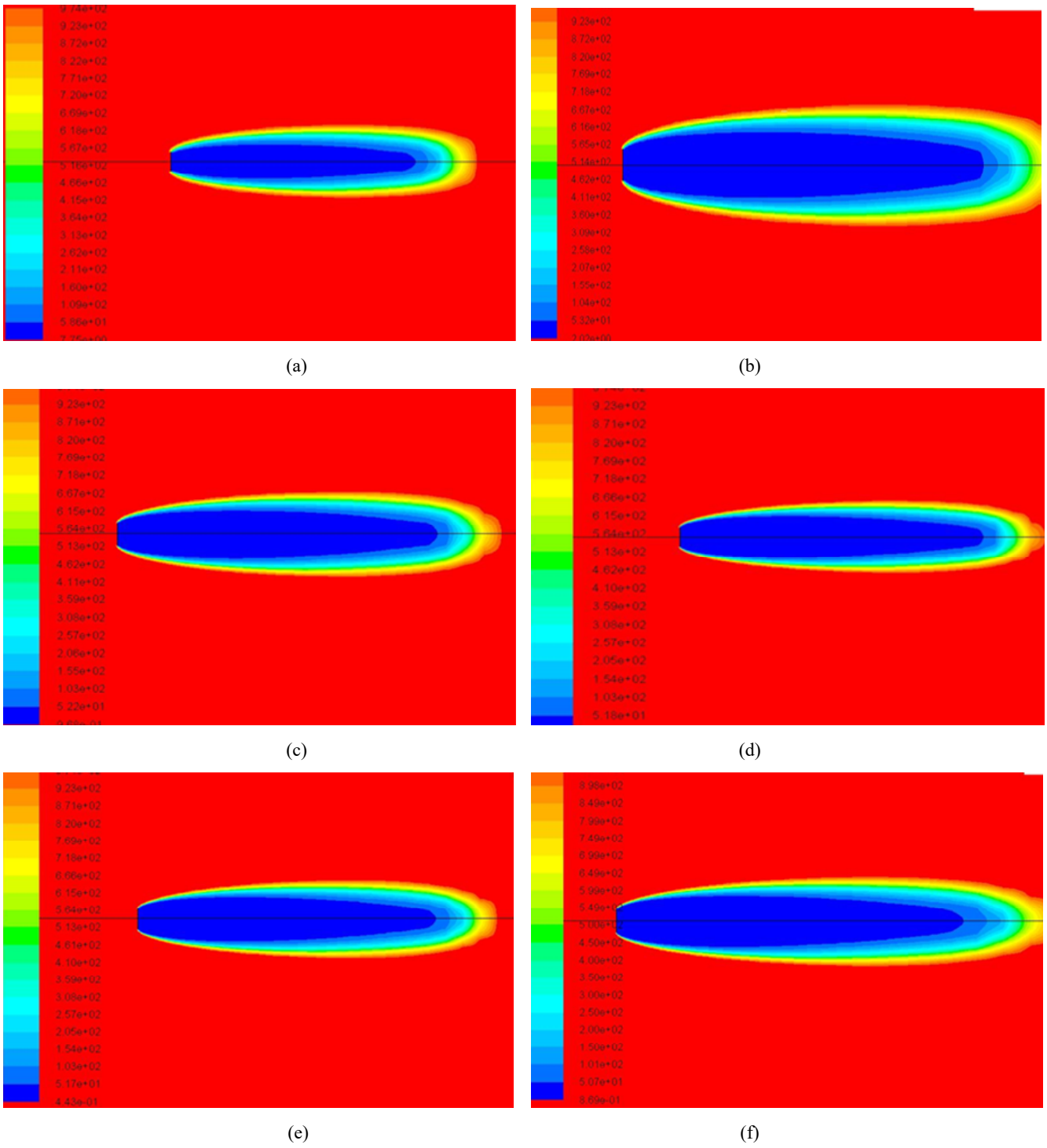

(a) (b)

(c) (d)

(e) (f)

Figure 7 Vapour density formation (mixture) for disk cavitator without projectile body (a) vapour density formation for 1 mm D_c (b) vapour density formation for 2 mm D_c (c) vapour density formation for 3 mm D_c (d) vapour density formation for 4 mm D_c (e) vapour density formation for 5 mm D_c (f) vapour density formation for 6 mm D_c (g) vapour density formation for 7 mm D_c (h) vapour density formation for 8 mm D_c (continued) (see online version for colours)

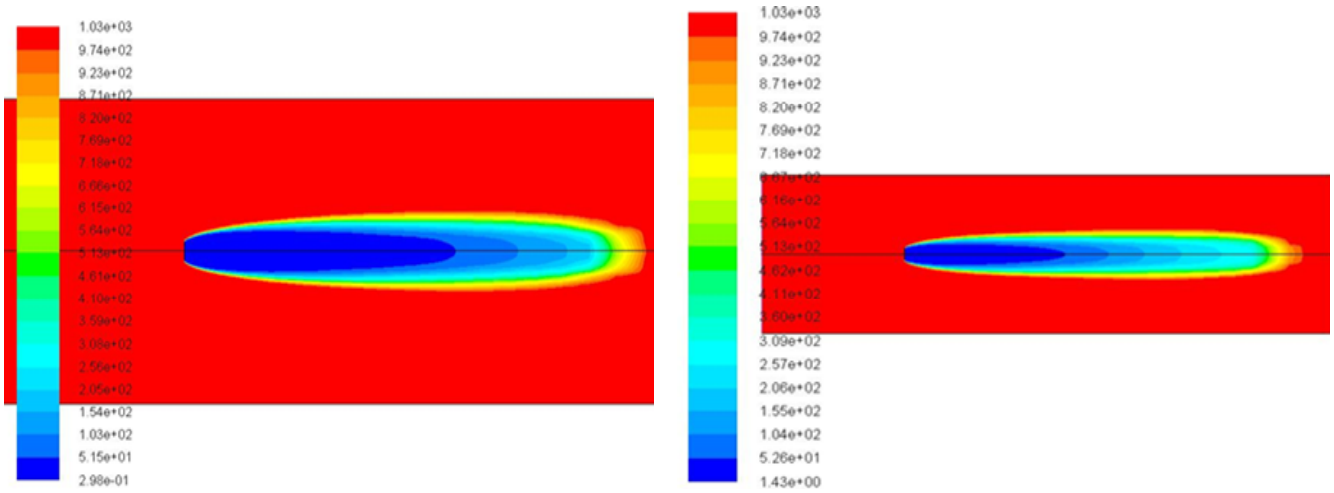

(g) (h)

It is clearly evident from the Figure 7(a) to Figure 7(h) contour that inside the two low-pressure vortices created, cavitation begins in the isolated flow area behind the disk. As the supercavity zone develops, pressure does not decrease, remaining stable at the vapour pressure.

Figure 8 Coefficient of drag value for cavitator disk diameter varying from 1 to 8 mm

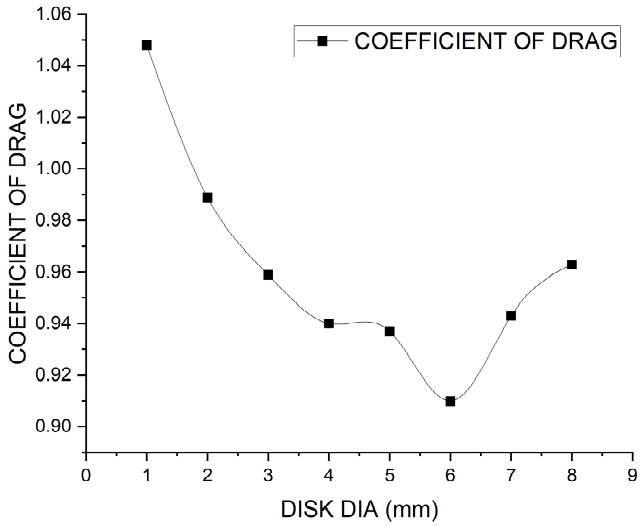

It can be noticed that there is variation in the vapour cavity creation that includes supercavity length and maximum cavity diameter according to the diameter of the disk cavitator. For a 1–5 mm cavitator, the vapour density obtained decreases, as represented in Figure 7(a) to Figure 7(e). Therefore, there is a decrease in skin fraction drag while pressure drag increases; at a specific point, the disk diameter attains the value of 6mm, that is, Figure 7(f). The vapour density is very low, resulting in a very low skin fraction and this is the reason the total drag of the object decreases, as represented in Figure 8. From the outcomes, the vapour density obtained approximately for a 6 mm cavitator is 0.9 kg/m^3 for the water density of 1,000 Kg/m^3 at an atmospheric pressure of 1 atm. As shown in Figure 7(g) to Figure 7(h), if the disk diameter rises further, from 7 mm–8mm, then the skin friction becomes less while the pressure drag increases, increasing the total drag of an object. Contour density information for visualising the envelope the data for cavitator is shown in Figure 7(i). As obtained from the simulations Figure 7(a) to Figure 7(h), the cavity length and cavity diameter increase if there is an increase in the disk diameter.

It is possible to calculate the aerodynamic drag force acting on an object in terms of viscous and pressure drag forces. In the case of bluff bodies, streamlining is generally not a feasible solution to reduce the drag because the selection of the bluff shape is frequent in the cavitator's design. Pressure drag has dominance for bluff bodies, and as evident from Figure 8, the C_D value varies in accordance with the disk diameter, pressure, and skin friction changes. When the diameter of the disk is 6 mm, C_D is low, as vividly noticed from the C_D trends.

4.2 Case 2: cone cavitator with projectile body

The analysis is carried out using a cone cavitator with projectile, having diameter of 8mm. Initially, the analysis is carried out using the velocity of 44m/s for the cavitation number k = 0.1. The cut section of the cone cavitator is taken into account for the analysis, and the Reynolds number considered for the analysis is Re = 1.58106 × 10^6. The atmospheric or operating pressure condition is 1 atm. Multiphase analysis is used by enabling the cavitation mechanism in the ANSYS Fluent software, and the flow is accelerated over the surface of the cone cavitator. From the cone cavitator analysis, it is observed that, the nose of the localised region does not initiate the flow separation over the surface of the cone with the projectile. It seems that the

vapours pocket formation is very less if the cavitator nose diameter is neglected, eventhough enabling the cavitation model due to cone shape, it act as a conventional Projectile. The drag of the cone cavitator is high due to less formation of the vapours pocket around the body. This shape does not fulfil the formation of supercavitation, so skin friction drag for this type of cavitator is high; hence, the total drag of the projectile is increasing. If this total drag is increasing, the coefficient of drag also gets increased, and the coefficient of drag for the analysis is 1.19 due to viscous drag effect in the analysis. The vapour density for the cone cavitator analysis is 3.452 kg/m^3 .The cone cavitator analysis is shown in Figure 9, and from this analysis, it is clear that, if the nose of the disk is negligible, there is an increase in the viscous effect .To reduce the viscous effect and increase in total drag, the nose of the cone is optimised with varying diameter, and that is detailed in the case 3.

Figure 9 Vapour density contour for cone cavitator analysis for the cavitation number 0.1 (see online version for colours)

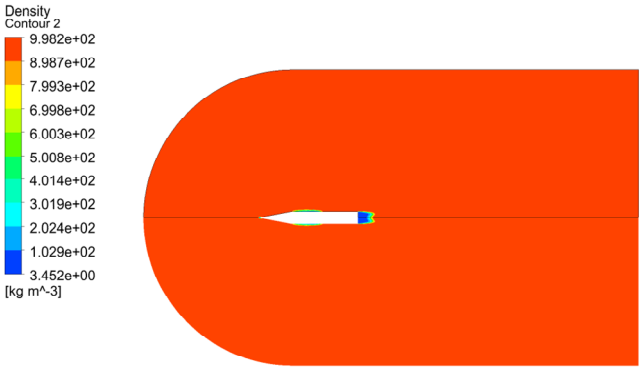

Figure 10 Vapour cavity formation for projectile with disk cavitator (a) vapour density formation for 1 mm D_c with projectile (b) vapour density formation for 2 mm D_c with projectile (c) vapour density formation for 3 mm D_c with projectile (d) vapour density formation for 4 mm D_c with projectile (e) vapour density formation for 5 mm D_c with projectile (f) vapour density formation for 6 mm D_c with projectile (g) vapour density formation for 7 mm D_c with projectile (see online version for colours)

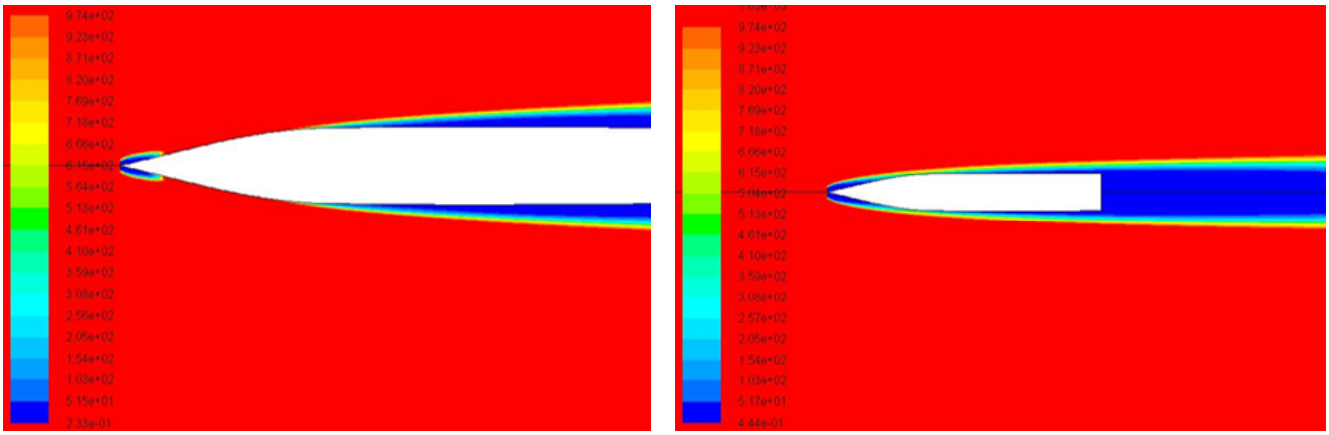

(a) (b)

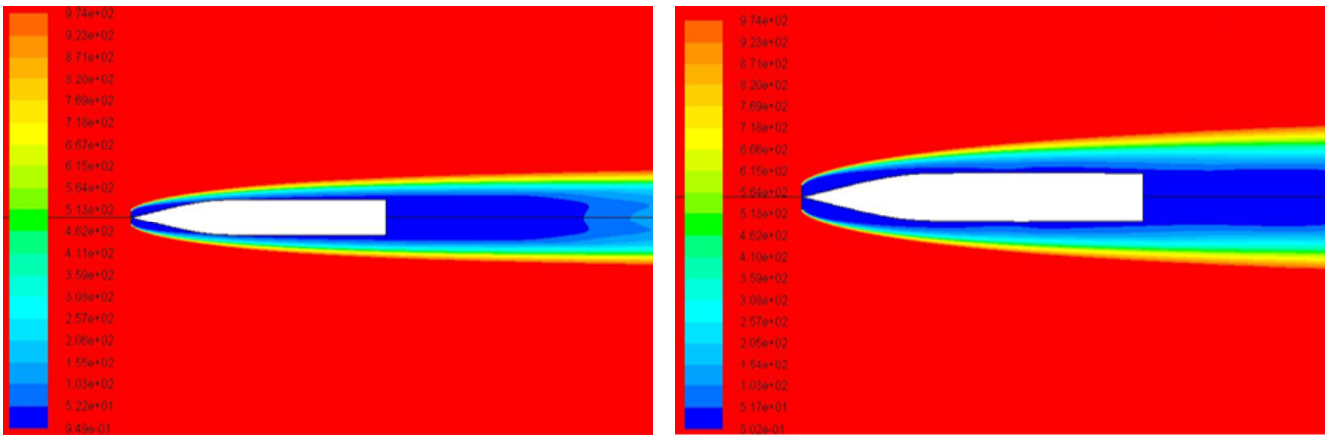

(c) (d)

Figure 10 Vapour cavity formation for projectile with disk cavitator (a) vapour density formation for 1 mm D_c with projectile (b) vapour density formation for 2 mm D_c with projectile (c) vapour density formation for 3 mm D_c with projectile (d) vapour density formation for 4 mm D_c with projectile (e) vapour density formation for 5 mm D_c with projectile (f) vapour density formation for 6 mm D_c with projectile (g) vapour density formation for 7 mm D_c with projectile (continued) (see online version for colours)

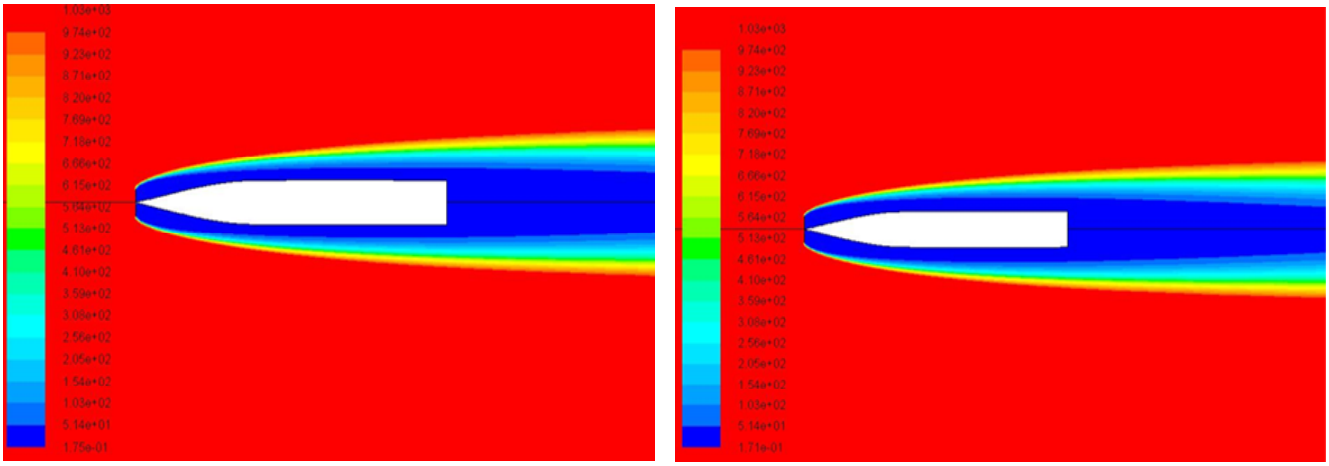

(e) (f)

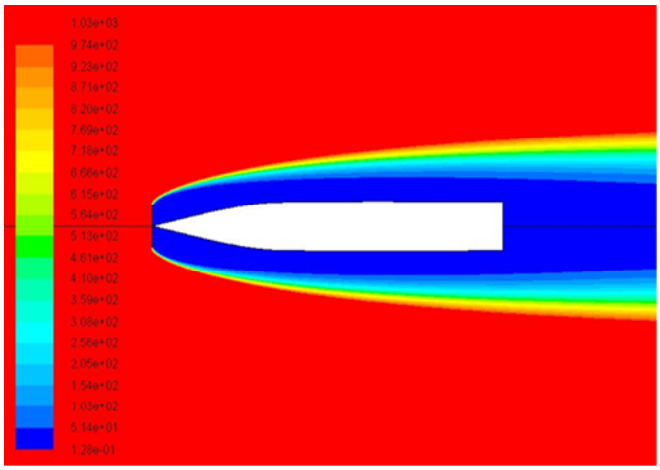

(g)

4.3 Case 3: optimisation of disk cavitator with projectile body

Further analysis is carried out using a disk with a projectile body; the cut section of the disk behind the body of the projectile is taken into account for the analysis and for the cavitation number ranging from 0.1 to 0.01 and for the Reynolds number Re = 1.58106×10^6 to 5.11106×10^6. A second-order upwind scheme is employed in carrying out CFD simulation. The flow is accelerated in the local zones around the nose when the projectile travels through the water at a sufficient pace, resulting in a drop in local pressure below the vapour pressure and hence forming a vapour cavity. On the other hand, a cavity can be generated, enveloping the body entirely, by having adequate speed and appropriate design features, namely a conical body and a flat nose tip, causing a low-drag projectile. A cavitator diameter with ten distinct cavitation numbers is taken into consideration for the optimisation of the projectile. The values of cavity length, cavity diameter, pressure drag, skin friction, and the total drag value are calculated from the simulation for each cavitation number. The coefficient of drag values of projection, with disk cavitation diameter varying for the cavitation number 0.01, are taken into account for comparing the simulation, and Figure 10(a) to Figure 10(h) represent the development of supercavity generation and cavity flow contour for various cavitator diameters with the projectile body. Vapour density contour colour coded information for visualising the envelope data for cavitator with projectile is shown in Figure 10(i). The momentum is spread across an expanding area as it is flowing downstream; thus, in the case of the disk, the greater axisymmetric divergence of the free surface after isolation may also have had an effect (Brennen, 1970). The natural cavitation is accomplished on the projectile body in the simulation with the aid of cavitation. Figure 10(a) depicts the vapour cavity beginning, and low cavity generation encloses a 1mm cavitator disk, resulting in high skin friction drag and high total drag as well.

In contrast, Figure 10(b) represents that when the vapour cavity initiates and tries to enclose the projectile's body, there is a drop in skin friction drag, hence reducing the total drag. It is clearly witnessed from Figure 10(c) that the vapour cavity encloses the projectile's body entirely, and the skin friction drag decreases, so the total drag reduces. Figure 10(d) to Figure 10(h) show that there are vapour pockets surrounding the body, reducing the skin friction drag. Even though the skin friction drag reduces, there is an increase in the pressure drag, and this is why [Figure 8(d) to Figure 8(h)] the total drag of a projectile increases, simultaneously increasing the cavity length, maximum cavity diameter, and coefficient of drag. Because of the variations in the disk diameter, the variation in C_D happened, as obtained from the simulation.

For a cavitator disk diameter of 3mm behind the projectile, the C_D value is lower. As represented in Figure 11, from the simulation plotted as a graph, the coefficient of drag value for two different cavitations and Reynolds numbers is obtained. This C_D value has an association with skin friction and pressure drag, and boundary layer development causes friction and pressure drag caused by eddying motions that the passage of the body sets up in the fluid. Here, the body with a 3mm cavitator disk is streamlined, and super-cavitation results in skin friction, which is substantially low.

Figure 11 Total drag coefficient for varying disk diameter with projectile for varying cavitation number (see online version for colours)

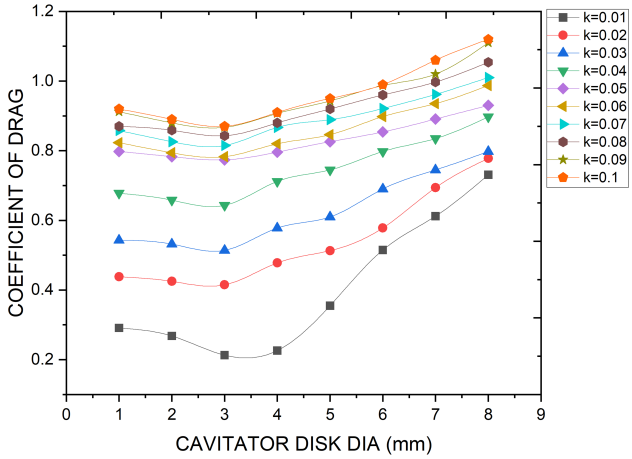

4.4 *Model validation*

The outcomes of the CFD simulation are put into comparison with the outcomes of the experiment conducted by Brennen (1970). There is steady flow generation evident in the experiment.

Based on the results obtained from Brennen (1969, 1970), the head form disk diameter was fixed. The dashed line in the Figure 12 illustrates the resulting value, which is given by Brennen (1970) for the cavitation number, and from the CFD simulation, the remaining solid line is obtained for the supercavitation number, k = 0.01, 0.02, 0.03, 0.04, 0.05, 0.06, 0.07, 0.08, 0.09, 0.1. Results obtained from the analysis are close to Brennen's (1969) values, and Figure 12 represents the comparison.

Figure 12 Plot between cavitator disk to projectile diameter vs. C_D (see online version for colours)

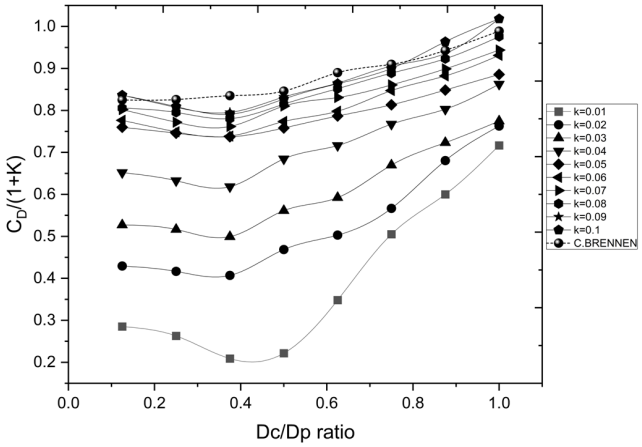

Further, it is evident from Figure 13 and Figure 14 that comparison is made for the cavitation length and maximum cavity diameter for the cavitation number (varying in nature) for the disk behind the projectile, and that is predicted from the findings of Garabedian (1956). Figure 15 depicts that the cavitation number, i.e., K = 0.1, is considered, and for the disk cavitator alone, the values are calculated for cavity length, maximum cavity diameter, and coefficient drag.

Figure 13 Plot between disk diameter vs. cavity length for k = 0.1 to 0.01 (see online version for colours)

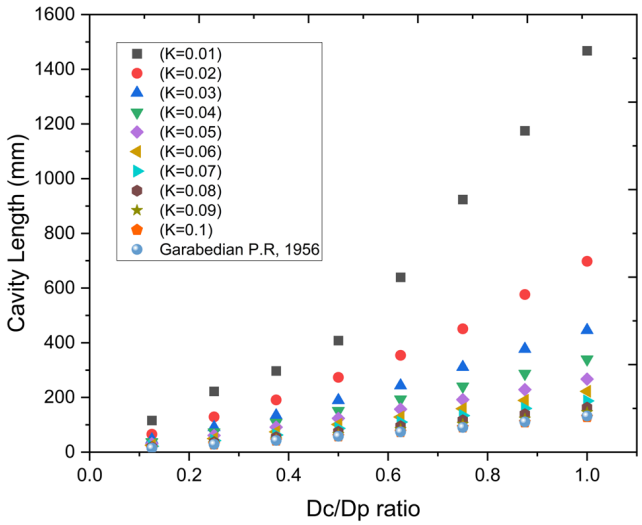

Garabedian (1956) carried out calculations for the dimensions of the cavity. His hypothesis was developed employing asymptotic relations while assuming a constant, axially symmetric, irrotational flow of an incompressible liquid. This model represents an assumption for the cavity with a symmetrically shaped nose and tail. From the outcomes, it is clear that if there is an increase in the diameter of the disk, the viscous effect is decreased, and pressure drag has an effect. Cavity length and cavity

diameter act as a function of cavitation number, and these values increase if the disk diameter increases, and it is predicted that they are directly proportional to the disk diameter.

Figure 14 Plot between disk dia vs. max cavity diameter for $k = 0.1$ to 0.01 (see online version for colours)

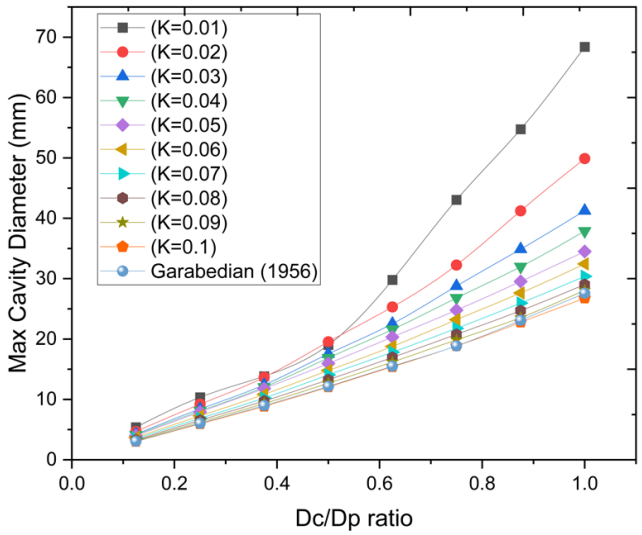

The length of the natural cavity obtained for all the disk diameters is depicted in Figure 15, and a plot is drawn for disk diameter against the difference in cavity pressure, and comparison is made with the existing results from Brennen (1969).

Figure 15 Plot between disk dia vs. cavity length, maximum cavity and C_D

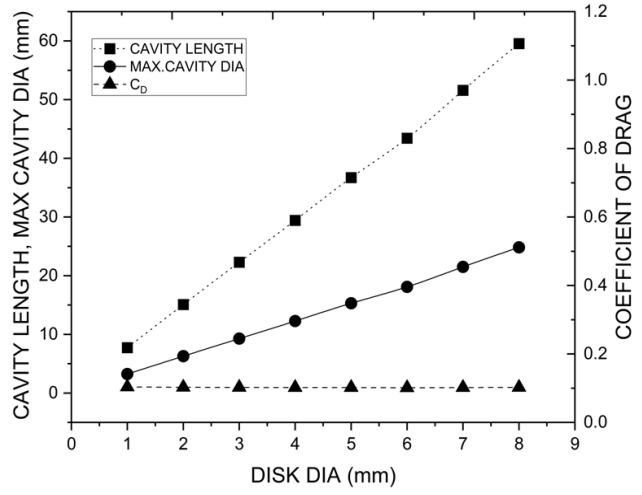

This plot shows a continuous increase in the cavity length, and the maximum cavity diameter rises with the increasing diameter of the disk.

A cavity closure point is also predicted and then compared with the outcome obtained from Brennen (1969) in order to maintain the vapour cavity, and that is represented in Figure 16 as a schematic diagram, where the dashed line indicates the result obtained by Brennen (1995) and the solid line is obtained from the computational analysis. In Figure 17, employing simulation results, the generation of the supercavity around the projectile due to the free stream line, smooth flow detachment, and cavity closure point are marked. The momentum is diffused across a spreading area as it is convected downstream; hence, in the case of the disk, the increased axisymmetric divergence of the free surface after isolation may also have had an effect. The hypothetical curve deviates from reality at the point named 'transition point'. Yet, it must always be taken into account that the transition never occurs at a particular point, and the term 'transition' itself is arbitrary (Sato and Kuriki, 1961).

Figure 16 Schematic diagram of cavity behind cavitator disk

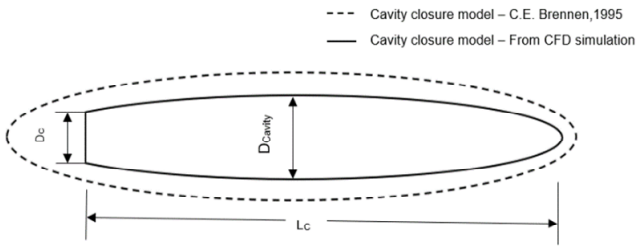

Figure 17 Free streamline analysis Cavity closure model – CFD simulation (see online version for colours)

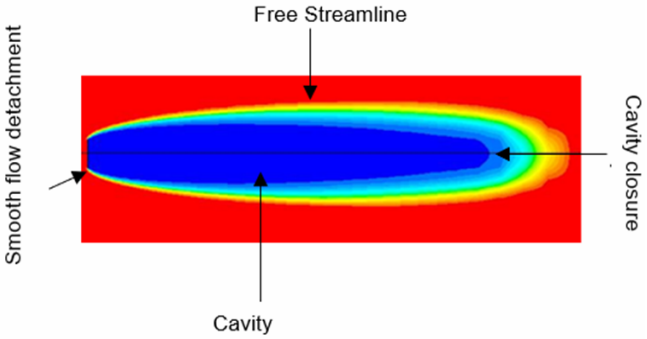

Figure 17, as follows, illustrates a more thorough description of the distribution of density in the transition zone. This paper considers three-dimensional projectiles with no heat transfer. The dashed line in Figure 16 depicts the free streamline analysis of Brennen (1995), and the solid line is obtained from the CFD simulation, as represented in Fig. 16 and 17. From this simulation, it is noticed that the cavity closure point is not linked to the solid body, and it is entire, enveloping the length of the projectile given.

- From the analysis its clearly observed that a super-cavitating high speed projectile's overall structure is considerably affected by the size of the caviator.
- First of all, a large cavitator results in a more sturdy and aerodynamically shaped front end, which is crucial for the penetration of the water and the beginning of the supercavity. The result of this is obtaining a projectile that is more hydrodynamically efficient and streamlined.
- Second is, the creation and maintenance of the supercavity is guaranteed by a right sized cavitator,

which decreases drag forces, allowing faster underwater velocities. However, a cavitator, that is undersized, may find it demanding to form a stable supercavity, potentially resulting in a rise in drag and reduced overall performance.

Finally, the stability and flow properties are influenced by the size of the cavitator, which affects the weight distribution of the projectile as well.

5 Conclusions

Simulation for super-cavitating flow past the disk cavitator and disk behind the projectile, simulation of flow employing FLUENT has been carried out. First and foremost, the simulation showed the stability and formation of a clearly defined supercavity, illustrating how effective the disk cavitator is in establishing a stable gas-filled zone surrounding the underwater object.

1 Behind the 3D disk cavitator, a supercavitator is developed that encases the projectile entirely.

2 The analysis depicts that if there is an increase in the diameter of the disk cavity, the geometry of the cavity, including supercavity length and maximum cavity diameter, also increases.

3 The result suggests that the supercavity length and maximum diameter are directionally proportional to the cavity's diameter.

4 The total drag of the projectile with cavitator is 12% if the disk diameter is 3 mm, when compared with the experimental results.

5 Even though there is an increase in pressure drag, there is a reduction in skin friction drag, so total drag is decreased for 1 m of seawater.

6 It is a demanding task to optimise the cavitator diameter, which plays a key role in the generation of super-cavitation. A better and minimal drag value is provided by a 3 mm cavitator disk diameter with a disk-to-projectile diameter ratio of 0.375.

7 Moreover, the analysis displayed the details about the pressure distribution in the supercavity, focussing on the low pressure regions that are perfect for the reduction of drag forces.

8 Finally, the CFD analysis provided a valuable information about the flow characteristics, and the way disk cavitator affects the surrounding water's behaviour.

References

Ashok, K.S., Mahesh, M.A., Huiying, L. and Yu, J. (2002) 'Mathematical basis and validation of the full cavitation model', *J. Fluids Eng*, Vol. 124, No. 3, pp.617–624.

Brennen, C. (1969) 'Some viscous and other real fluid effects in fully developed cavity flows', *Cavitation State of Knowledge, ASME*, Vol. 44, No. 1, pp.51–63.

Brennen, C. (1970) 'Cavity surface wave patterns and general appearance', *J. Fluid Mech.*, Vol. 44, Part 1, pp.33–49.

Brennen, C.E. (1995) *Cavitation and Bubble Dynamics*, Oxford University Press, Oxford.

Chang, X., Jian, H., Yiwei, W., Xiaocui, W., Chenguang, H. and Xianqian, W. (2018) 'Supercavitating flow around high-speed underwater projectile near free surface induced by air entrainment', *AIP Advances*, Vol. 8, No. 3, p.035016.

Chou, Y.S. (1974) 'Axisymmetric cavity flows past slender bodies of revolution', *Journal of Hydronautics*, Vol. 8, No. 1, pp.13–18.

Dong-Hui, Z., Hong-Hui, S. and Hui-Xia, J. (2022) 'Characteristics of the multiphase flow field with super-cavitation induced by successively fired projectiles under-water and cross-medium', *Journal of Mechanical Science and Technology*, Vol. 36, No. 1, pp.247–258.

Gadd, G.E. and Grant, S. (1965) 'Some experiments on cavities behind disks', *J. Fluid Mech.*, Vol. 23, Part 4, No. 4, pp.645–656.

Garabedian, P.R. (1956) 'The mathematical theory of three-dimensional cavities and jets', *Bull. Amer. Math. Soc*., Vol. 62, No. 2, pp.219–235.

Gugulothu, S.K. (2020) 'Computational modeling on supercavitating flow over axisymmetric cavitators', *Ocean Engineering*, 15 August, Vol. 210, pp.107515.

Hrubes, J. (2001) 'High-speed imaging of supercavitating underwater projectiles', *Experiments in Fluids*, Vol. 30, No. 1, pp.57–64.

Jagadeshwar, K.P., Usha S.P., Ravinder, R. and Gugulothu, S.K. (2021) 'Numerical and experimental evaluation of nearwake cavitation flow around axisymmetric cavitators', *Ships and Offshore Structures*, Vol. 17, No. 5, pp.1042–1052.

Knapp, R., Daily, J. and Hammit, F. (1970) *Cavitation*, McGraw-Hill Book Comp., New York.

Ko, D.R.S., Kubota, T. and Lees, L. (1969) 'Finite disturbance effect on the stability of a laminar incompressible wake behind a flat plate', *Journal of Fluid Mechanics*, Vol. 40, No. 2, pp.315–341.

Kunz, R.F., Stinebring, D.R., Chyczewski, T.S., Boger, D.A., Gibeling, H.J. and Govindan, T.R. (1999) 'Multi-phase CFD analysis of natural and ventilated cavitation about submerged bodies', *Proceedings of the 1999 3rd ASME/JSME Joint Fluids Engineering Conference*, FEDSM'99, San Francisco, California, USA.

Lotan, A.L. and Alon, G. (2022) 'Experimental study of supercavitation bubble development over bodies in a free-surface flow', *J. Mar. Sci. Eng.*, Vol. 10, No. 9, p.1244.

Patankar, S.V. (1980) *Numerical Heat Transfer and Fluid Flow*, Hemisphere Publishing Corporation, Washington.

Peter, J.K.C., Peter, H.R., John, W.D. and David, H.G. (2011) 'An experiment for the study of free-flying supercavitating projectiles', *J. Fluids Eng.*, Vol. 133, No. 2, p.021303-9.

Salil, S.K. and Rudra, P. (2000) 'Studies on the dynamics of a supercavitating projectile', *Applied Mathematical Modelling*, Vol. 24, No. 2, pp.113–129.

Sato, H. and Kuriki, K. (1961) 'The mechanism of transition in the wake of a thin flat plate placed parallel to a uniform flow', *J. Fluid Mech.*, Vol. 11, No. 3, pp.321–352.

Seongjin, H. and Gihun, S. (2021) 'Numerical simulation of cavitating flows around an oscillating circular cylinder', *Ocean Engineering*, 15 April, Vol. 226, pp.108739.

Tassinleger, A. and Ceccio, S.L. (1998) 'Examination of the flow near the leading edge of attached cavitation. Part 1. Detachment of two-dimensional and axisymmetric cavities', *J. Fluid Mech.*, Vol. 376, No. 1, pp.61–90.

Van-Duyen, P., Ji-Woo, H., Ali, K.H., Kiseong, K. and Byoung-Kwon, A. (2022) 'Experimental investigation of ventilated supercavitation behind cone-shaped with different angles and disk-shaped cavitators', *International Journal of Naval Architecture and Ocean Engineering*, 15 December, Vol. 14, Part 3, p.112921.

Van-Tu, N. and Warn-Gyu, P. (2022) 'Numerical study of the thermodynamics and supercavitating flow around an underwater high-speed projectile using a fully compressible multiphase flow model', *Ocean Engineering*, p.257.

Yao-Tsu, W.T. and Wang, D.P. (1963) 'A wake model for free-streamline flow theory, part 2. Cavity flows past obstacles of arbitrary profile', *J. Fluid Mech.*, Vol. 18, No. 1, pp.65–93.